THE ASTROPHYSICAL JOURNAL, 426:563–576, 1994 May 10

PROBING THE GALACTIC DISK AND HALO. I. THE NGC 3783 SIGHT LINE[1]

LIMIN LU,[2] BLAIR D. SAVAGE,[2] AND KENNETH R. SEMBACH[3,4]

Received 1993 September 7; accepted 1993 November 12

ABSTRACT

We report a study of Galactic disk and halo absorption toward the Seyfert galaxy NGC 3783 which has Galactic coordinates $l = 287.46$ and $b = +22.95$. The data were obtained with the Goddard High Resolution Spectrograph operating at medium resolution with the Large Science Aperture, which produces a line spread function having a sharp core (FWHM ~ 20 km s^{-1}) and broad wings extending to ± 70 km s^{-1}. Ion species detected in absorption near zero LSR velocity include C IV and N V for high ions, and C I, Mg II, Si II, and S II for low ions. Absorption from a high-velocity cloud (HVC) at a velocity of $+240$ km s^{-1} along the sight line is also detected in the ion species of S II, Si II, and probably C I. This is the first reported case where S II and C I absorption has been detected in a HVC. The S II lines are especially useful since metal abundance estimates based on S are largely unaffected by dust grains. The study is aided by the availability of 21 cm emission data. The main results are the following:

1. The integrated high ion column densities are log N(N V) $= 13.55 \pm 0.12$ and log N(C IV) $= 14.30 \pm 0.03$. These values are consistent with the high ions being produced in the gas of a galactic fountain cooling from temperatures exceeding 2×10^5 K.
2. The C IV absorption toward NGC 3783 exhibits an asymmetric extension to large positive velocity. The C IV profile is roughly modeled by a corotating absorbing gas with an exponential scale height of 3.5 kpc. This scale height estimate is similar to the 4.4 kpc value found for the direction of the Large Magellanic Clouds and also agrees with the C IV scale heights determined from the $N|\sin b|$ versus $|z|$ analysis technique.
3. For the intermediate velocity gas at $+62$ km s^{-1} toward NGC 3783 we estimate an approximate S abundance of 0.5 ± 0.2 times the solar value. The abundance measurement may be influenced by differences in sampling geometry as it relies on a H I column density based on 21 cm data obtained with a large radio beam. The S abundance is consistent with that expected from the known metallicity gradient in the Galactic disk if the intermediate velocity gas is a corotating high-z extension of an outer spiral arm of the Galaxy at a Galactocentric distance of ~ 14 kpc. The implied z distance of the gas is ~ 5 kpc.
4. For the HVC at $+240$ km s^{-1}, the unsaturated S II lines result in a S abundance of about 0.15 ± 0.05 times the solar value. The estimate may be affected by differences in sampling geometry between the UV and radio data that were used to derive the H I column density. Based on the velocity and the S abundance of the HVC, we conclude that the HVC is most likely associated with gas being stripped away by the Galaxy from an extragalactic object, such as the Magellanic Clouds or some other member of the Local Group. Such a phenomenon may have significant implications for the study of quasar absorption line systems.

Subject headings: cooling flows — galaxies: individual (NGC 3783) — galaxies: Seyfert — Galaxy: halo — infrared: ISM: lines — ISM: abundances

1. INTRODUCTION

The possible existence of a hot (10^5–10^6 K), extended gaseous halo surrounding the Galactic disk (Shklovsky 1952; Spitzer 1956) was confirmed by observations of highly ionized ion absorption (e.g., Si IV, C IV, and N V) in the ultraviolet with the *IUE* satellite toward bright stars in the LMC and the SMC (Savage & de Boer 1979, 1981; Fitzpatrick & Savage 1983; Savage et al. 1989), and toward distant halo stars (Pettini & West 1982; Savage & Massa 1987). These studies suggest that highly ionized gas exists far above and below the Galactic disk, with an exponential scale height of $\sim$3–5 kpc (Sembach & Savage 1992; Savage et al. 1993a). The exchange of energy, momentum, and metal-enriched gas between the disk and halo may have a significant influence on Galactic evolution. Detailed reviews of the subject may be found in Savage (1988), Spitzer (1990), and McKee (1993).

To understand fully the extent, structure, kinematics, chemical and physical states of the gaseous Galactic halo, one must be able to probe its entire spatial extent. Such studies require ultraviolet observations toward extragalactic objects, which were rare prior to the era of *HST* because the *IUE* satellite can produce high-quality spectra only for relatively bright targets. In fact, high-quality, high-resolution *IUE* observations toward extragalactic objects have until recently only existed for a few stars along the LMC and the SMC sight lines, and for several spectral lines toward 3C 273 (Burks et al. 1991). The recent observations of the quasar 3C 273 (Savage et al. 1993b) with the medium resolution gratings of the Goddard High Resolution Spectrograph (GHRS) on board the *HST* has revealed the importance of probing the entire extent of the gaseous Galactic halo.

[1] Based on observations with the NASA/ESA *Hubble Space Telescope*, obtained at the Space Telescope Science Institute, which is operated by the Association of Universities for Research in Astronomy, Inc., under NASA contract NAS 5-26555.

[2] Washburn Observatory, University of Wisconsin, 475 N. Charter Street, Madison, WI 53706.
[3] Center for Space Research, Building 37, Massachusetts Institute of Technology, Cambridge, MA 02139.
[4] Hubble Fellow.

In this paper we present the first of a series of studies designed to investigate the properties of hot Galactic disk and halo gas using observations of absorption by highly ionized species toward bright quasars/AGNs and distant halo stars. The observations were carried out with the GHRS on board the *HST*. The target in this study is NGC 3783, a Seyfert 1 galaxy at a redshift of $z_{em} = 0.0096$ (Weedman 1976). With a visual magnitude of ~ 13 (somewhat variable), NGC 3783 is one of the brightest Seyfert galaxies in the sky. Its nucleus provides a smooth power-law spectrum that can be effectively used to probe absorption by intervening material along the sight line, including the disk and halo of the Seyfert galaxy itself and that of the Milky Way. Our interest in NGC 3783 is enhanced by its fortuitous location ($l = 287.46$, $b = +22.95$) behind a high-velocity cloud (HVC) denoted HVC 287.5+22.5+240, which is part of a complex of high positive velocity clouds possibly related to the well-known Magellanic Stream (Mathewson, Cleary, & Murray 1974; Hulsbosch 1975). West et al. (1985) have detected Ca II absorption from that HVC at a local standard of rest velocity $v_{LSR} \sim +240$ km s^{-1}. The GHRS spectra we analyze ($\lambda = 1233$–1268 Å and 1528–1562 Å) cover not only the N V and C IV doublets, but also low-ionization species of S II $\lambda\lambda$1250.584, 1253.811, 1259.519, Si II λ1260.422, and C I λ1560.309. This will allow us to study the metal abundances in the HVC.

The paper is organized in the following way: In § 2 we describe the data acquisition and calibrations, and absorption line measurements. The analysis of absorption near zero velocity is given in § 3 for the highly ionized species and in § 4 for low ion species. The absorption by the high-velocity cloud, both in high and low ions, is analyzed and discussed in § 5. The main results are summarized in § 6.

2. OBSERVATIONS, CALIBRATIONS, AND MEASUREMENTS

2.1. *Observations and Reductions*

The observation was carried out on 1993 February 21 with the GHRS on board the *HST*. The detailed characteristics of the GHRS are described in Duncan (1992). The medium resolution grating G160M was used with the Large Science Aperture (LSA) to cover the wavelength range 1233–1268 Å. The total exposure time was 7983 s, with $\sim 11\%$ spent on measuring the detector background using the 500 Digicon science diodes. A platinum-neon lamp exposure was also taken for wavelength calibration purposes. All spectral observations were obtained with substep pattern 4, which provides two samplings per diode. Standard FP-split and four-diode comb-addition were performed in order to reduce the effects of fixed pattern noise on the photocathode and diode-to-diode sensitivity variation in the detector. The on-board Doppler compensation for correcting spacecraft motion was enabled during all observations. The initial processing of the data was carried out with the IDL-based GHRS reduction software (Robinson et al. 1992). The individual FP-split spectra were aligned and combined using the standard merge routine developed at the University of Wisconsin-Madison. The merged spectrum was then resampled to a linear wavelength scale with a sampling interval of $\Delta\lambda = 0.0361$ Å ($\Delta v \sim 8.6$ km s^{-1}, corresponding to roughly half a diode width) while preserving the total number of samples (1000) in the original spectrum.

The resulting spectrum is shown in Figure 1, along with the 1 σ noise spectrum. The wavelength is heliocentric in vacuum. The S/N per half-diode sampling interval varies from 12:1 near Si II λ1260.422 to 16:1 near N V λ1238.821. The spectrum shows obvious absorption by the Galactic disk and halo gas near zero velocity in N V λ1238.821, S II $\lambda\lambda$1250.584, 1253.811, 1259.519, and Si II λ1260.422. Weak absorption by N V λ1242.804 and Mg II λ1239.925 also appear to be present. In addition, we detect absorption by the HVC at $v_{LSR} = +240$ km s^{-1} in S II $\lambda\lambda$1250.584, 1253.811, and Si II λ1260.422. The HVC absorption of S II λ1259.519 is blended with the Si II λ1260.422 absorption near zero velocity. All lines are marked and labeled in Figure 1.

The pair of broad absorption lines at $\lambda = 1248.59$ and 1252.62 Å forms a N V $\lambda\lambda$1238.821, 1242.804 doublet at a redshift of $z = 0.00778$. Given the emission redshift $z_{em} = 0.0096$ for NGC 3783, this N V doublet is likely absorption arising

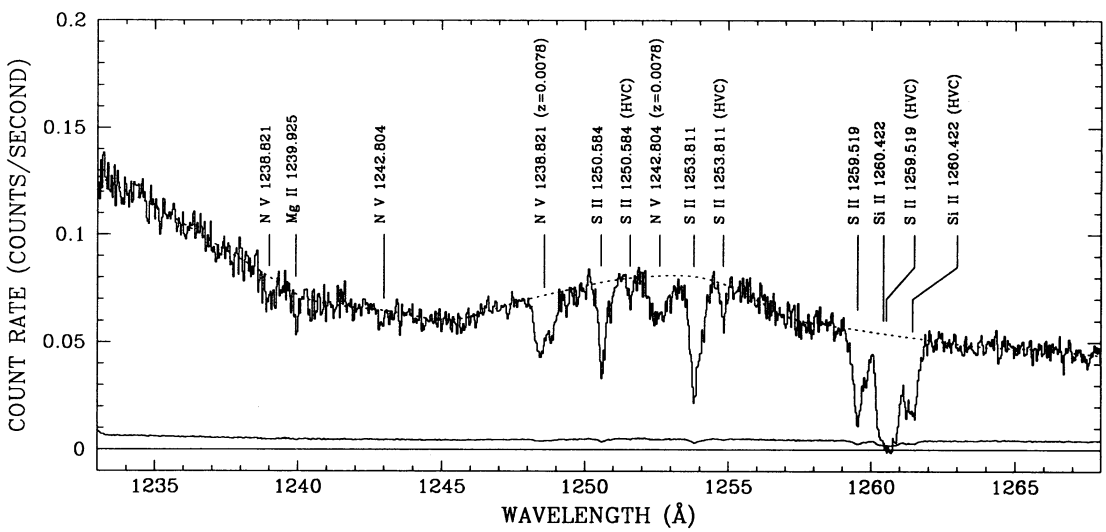

FIG. 1.—Spectrum of the Seyfert galaxy NGC 3783, obtained with the G160M grating and the GHRS. The lower spectrum is the 1 σ noise array. The adopted continuum is shown as the dotted line. Absorption lines are marked and labeled. In addition to Galactic disk and halo absorption near zero velocity, the spectrum also shows absorption by the HVC at $v_{LSR} = +240$ km s^{-1} along this sight line, and N V doublet absorption at a redshift $z = 0.00778$, which is most likely due to material somehow related with the Seyfert galaxy itself. The increase of flux toward shorter wavelength is due to the Lyα emission of the Seyfert galaxy, while the peak at $\lambda \sim 1252$ Å is due to the N V emission of the Seyfert galaxy.

from either regions surrounding the nucleus of the Seyfert galaxy, or from material in other galaxies that reside in the same cluster as NGC 3783 itself. Alternatively, the absorption may arise from an intervening galaxy along the line of sight that is totally unrelated with the Seyfert galaxy. Detailed analysis of this N v doublet absorption will be presented elsewhere (Maran et al. 1994).

2.2. *Additional Data*

The analysis discussed in the subsequent sections also involve GHRS G160M observations of C IV $\lambda\lambda$1548.195, 1550.770 and C I λ1560.309 absorption produced in the Galactic disk and halo toward NGC 3783. The data were kindly made available to us by S. Maran and collaborators (Maran et al. 1994). Details of that observation are given in the above reference. Very briefly, the instrument setup was similar to that described in § 2.1, except that substep pattern 5 was used, which gives four samplings per diode instead of two. The total integration time including ~6% on monitoring the background was 4093 s. The data were independently reduced by us in the same way as described in § 2.1. The final merged spectrum was then rebinned to a sampling interval of 0.0353 Å ($\Delta v \sim 6.8$ km s^{-1}), corresponding to half a diode width. The resulting spectrum has a S/N ~ 10:1 per half-diode sampling interval near the C IV doublet. Galactic absorption lines detected in this spectrum include the C IV doublet, C I λ1560.309, C I* λ1560.682, and C I** λ1561.438.

We note that the C IV λ1548.195 absorption corresponding to the $z = 0.00778$ N V absorption system should occur at an observed wavelength of 1560.24 Å, very close to the C I λ1560.309 absorption from the Milky Way disk gas. However, the corresponding C IV λ1550.770 absorption of the $z = 0.00778$ system should occur at an observed wavelength of 1562.83 Å, for which the Maran et al. (1994) spectrum shows no evidence at all. The 2 σ upper limits on the equivalent width of the C IV λ1550.770 absorption associated with the $z = 0.00778$ N V absorption system is 0.027 Å, implying a 2 σ upper limit of 0.054 Å for the corresponding C IV λ1548.195 absorption. Given the strength of the absorption line occurring near 1560.3 Å (see Table 1), we conclude that the absorption is primarily due to C I λ1560.309 associated with the Milky Way disk gas.

2.3. *Line Profiles and Equivalent Width Measurements*

In order to facilitate further analysis, the continuum for the spectrum shown in Figure 1 is established by fitting a cubic-spline function to regions in the spectrum that are free of obvious absorption lines. The resulting continuum is shown in Figure 1 as the dotted line superposed on the spectrum. A continuum is established in a similar fashion for the spectrum

TABLE 1

EQUIVALENT WIDTH MEASUREMENTS

Ion	λ[a] (Å)	f[a]	v_-[b] (km s^{-1})	v_+[b] (km s^{-1})	$\langle v_{LSR}\rangle$[c] (km s^{-1})	$W_\lambda \pm \sigma$ (Å)
Absorption Near Zero Velocity						
C I	1560.309	0.0804	−60	+50	+11	0.104 ± 0.017
C I*	1560.682	0.0603	−20	+20	+2	0.024 ± 0.008[d]
C I**	1561.438	0.0675	...	...	...	...[e]
C IV	1548.195	0.191	−80	+120	+24	0.494 ± 0.028
C IV	1550.770	0.0952	−80	+120	+30	0.310 ± 0.033
N V	1238.821	0.157	−60	+100	+26	0.070 ± 0.018
N V	1242.804	0.0782	−60	+100	+20	0.028 ± 0.023
Mg II	1239.925	0.000267	−60	+60	−2	0.044 ± 0.016
Si II	1260.422	1.01	−100	+160	+37	0.879 ± 0.014[f]
S II	1250.584	0.00545	−100	+140	+12	0.191 ± 0.025
S II	1253.811	0.0109	−100	+140	+10	0.345 ± 0.021
S II	1259.519	0.0162	−100	+120	+13	0.393 ± 0.022
Absorption by High-Velocity Cloud						
C I	1560.309	0.00804	+170	+290	+236	0.032 ± 0.019[e]
C IV	1548.195	0.191	...	...	...	<0.070[f]
C IV	1550.770	0.0952	...	...	...	<0.070[f]
N V	1238.821	0.157	...	...	...	<0.040[f]
N V	1242.804	0.0782	...	...	...	<0.040[f]
Si II	1260.422	1.01	+160	+340	+231	0.368 ± 0.018
S II	1250.584	0.00545	+160	+300	+240	0.026 ± 0.018
S II	1253.811	0.0109	+160	+300	+236	0.052 ± 0.018
S II	1259.519	0.0162	...	...	...	...[g]

[a] Rest-frame vacuum wavelength and oscillator strength from Morton 1991.

[b] v_- and v_+ give the LSR velocity range within which the equivalent width is measured.

[c] Absorption-weighted average LSR velocity for the absorption line.

[d] The C I* λ1560.682 absorption near zero velocity is blended with the C I λ1560.309 absorption at intermediate velocity near $v_{LSR} \sim +62$ km s^{-1}. The absorption has been assumed to be mostly due to C I* near zero velocity.

[e] The C I** λ1561.438 absorption near zero velocity is blended with the C I λ1560.309 absorption from the HVC at $v_{LSR} = +240$ km s^{-1}. The blended absorption is called "Feature A" and assumed to be mostly due to C I from the HVC.

[f] Limits are 2 σ, assuming the lines are unresolved.

[g] The S II λ1259.519 absorption from the HVC is blended with the Si II λ1260.422 absorption from the zero velocity gas. The absorption has been assumed to be mostly due to Si II from the zero velocity gas.

obtained by Maran et al. (1994), but reduced independently by us.

In Figure 2 we show the profiles of selected absorption lines (normalized to have unity continuum) with respect to local standard of rest (LSR) velocity. In the remaining analysis, all references of velocity are LSR values. In the direction of NGC 3783, the correction from heliocentric velocity to LSR velocity is given by $v_{LSR} - v_{helio} = -7.3$ km s^{-1}. Note that the profiles shown in Figure 2 aso include that of C IV $\lambda\lambda$1548.195, 1550.770 from Maran et al. (1994).

The absorption line profiles are significantly affected by the line spread function, which is shown in the top-left panel of Figure 2 for a well-centered point source. The spherical aberration of the *HST* primary mirror causes the line spread function in the LSA to have a sharp core surrounded by nearly symmetric broad wings. The core has a FWHM of about 1.2 diode widths ($\sim$20 km s^{-1} at 1250 Å and $\sim$16 km s^{-1} at 1550 Å) and contains about 40% of the area. The wings extend to roughly $\pm$4 diode widths ($\sim\pm$70 km s^{-1} at 1250 Å and $\sim\pm$55 km s^{-1} at 1550 Å), and contains the remaining 60% of the area. This information is important for understanding the details of the line profiles (see §§ 3.2 and 4.2).

In the top-right panel of Figure 2, we show the 21 cm emission profile in the velocity range $-200 < v_{LSR} < +300$ km s^{-1} toward NGC 3783. The 21 cm spectrum between $-200 < v_{LSR} < +200$ km s^{-1} was obtained by Danly, Lockman, & Savage (1994) with the NRAO 43 m radio telescope with a beam width of FWHM = 21′ at a velocity resolution of FWHM = 1 km s^{-1}. The data were corrected for antenna sidelobe contamination using the procedures outlined in

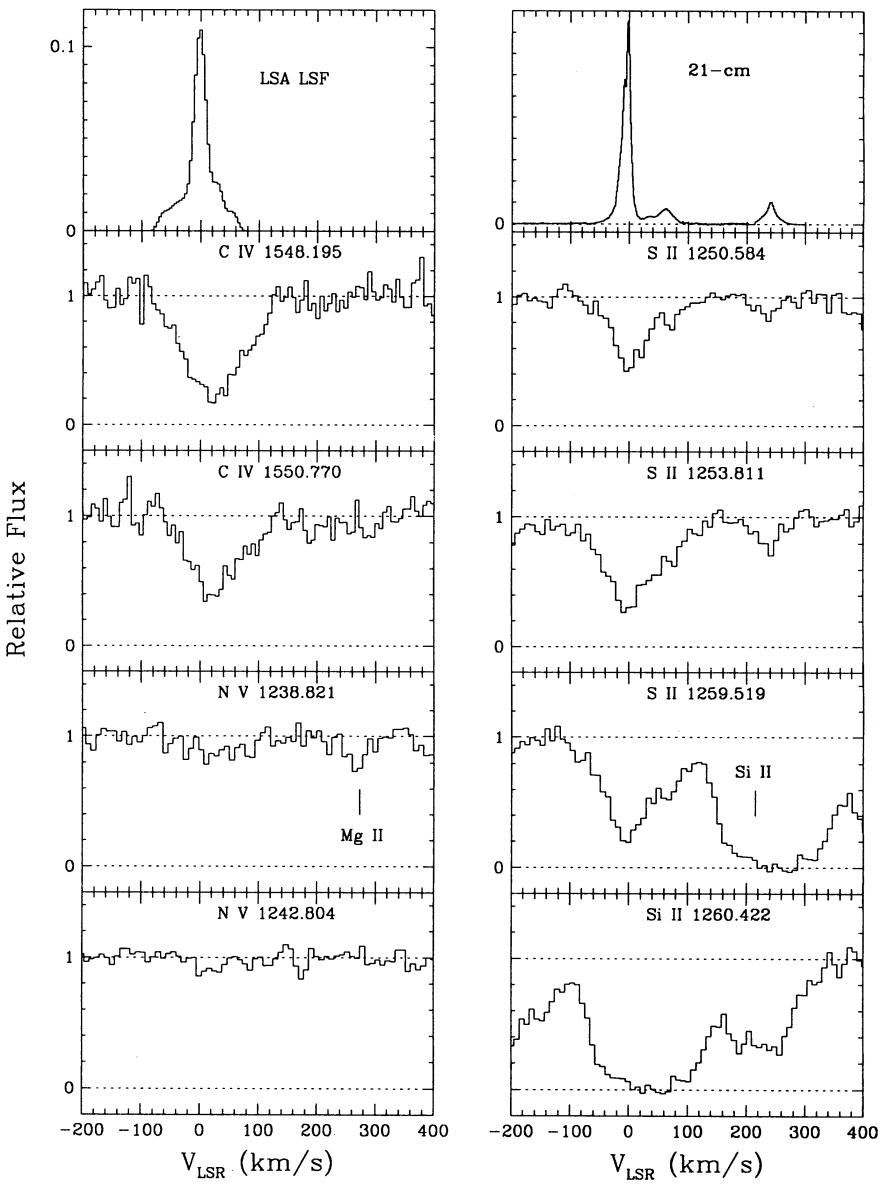

FIG. 2.—Normalized absorption profiles of selected lines detected in the spectrum of NGC 3783 (the C IV profiles are from Maran et al. 1994), plotted against LSR velocity. Absorption by the HVC at $v_{LSR} = +240$ km s^{-1} are detected in the three S II lines (one blended with the Si II λ1260.422 line near zero velocity) and in the Si II λ1260.422 line. The panel for N V λ1238.821 includes absorption by Mg II λ1239.925 (marked), while the panel for S II λ1259.519 includes Si II λ1260.422 absorption near zero velocity (marked). The top two panels show the line spread function (*left*) appropriate at 1250 Å for the G160M grating in the LSA, and the 21 cm emission profile (*right*) toward NGC 3783.

Lockman, Jahoda, & McCammon (1986). The 21 cm spectrum in the region $+200 < v_{LSR} < +300$ km s^{-1} is the *fit* using two Gaussian components to the data shown in West et al. (1985, see their Figure 4 and Table 4). This spectrum was obtained with a beam width of 34′ at a spectral resolution of 2 km s^{-1}. For convenience of discussion, we will refer to the main emission near -5 km s^{-1} (apparently showing two components) in the 21 cm profile as the "low velocity gas," and that near $+62$ km s^{-1} (including the small peak at $\sim +35$ km s^{-1}) as the "intermediate velocity gas." Sometimes the two above will be collectively referred to as "gas near zero velocity." The component near $+240$ km s^{-1} will always be referred to as the "high velocity gas" or the HVC.

Equivalent widths for all lines detected in our spectrum are given in Table 1, with the addition of the C IV doublet and the C I measurements. The first three columns of Table 1 list the ion name, vacuum wavelength, and oscillator strength from Morton (1991). All equivalent widths are measured from direct integration of the normalized spectrum within a specified LSR velocity range given by v_- and v_+, listed in columns (4) and (5) of Table 1. The resulting mean velocity of the absorption and the equivalent width are listed in columns (6) and (7), respectively. Uncertainties of the equivalent widths are calculated including both the contribution from photon-counting noise and from continuum-placement uncertainty (see Savage et al. 1993b and references therein).

2.4. *Absolute Wavelength Scales*

The absolute wavelength calibration of the GHRS spectra is accurate to within 1 diode (roughly 17 km s^{-1} at 1250 Å). Target centering in the LSA will affect the absolute wavelength scale, as well as the line spread function. Examination of the image map made at the time of target acquisition for the spectrum shown in Figure 1 indicates that the target was well centered in the LSA. The accuracy of the wavelength scale can be gauged independently from the HVC absorption features: the mean LSR velocity of the two well-separated S II HVC absorption lines (Table 1) is $+238$ km s^{-1}, which agrees very well with the values of $+241$ km s^{-1} from the Ca II HVC absorption, and $+240$ km s^{-1} from the 21 cm HVC emission line (West et al. 1985 and references therein). Thus, no further wavelength calibration of our spectrum is necessary.

The absolute wavelength scale of the spectrum obtained by Maran et al. (1994), containing the C IV doublet and the C I absorption, is uncertain. No image map was produced at the time of target acquisition. In order to tie the wavelength scale of this spectrum to that of ours shown in Figure 1, we compare in Figure 3 the absorption produced by Mg II λ1239.925 and S II λ1250.584, which occur in the spectrum shown in Figure 1, with that of C I λ1560.309, which occurs in the spectrum containing the C IV absorption. Both the weak Mg II and the C I lines should trace the high column density gas centered near -5 km s^{-1} in the 21 cm emission. The deepest part of the S II absorption lines should also coincide with the peak of the 21 cm absorption. Figure 3 shows that this is indeed the case. Thus, no further velocity adjustment for the C IV absorption is necessary.

3. ABSORPTION BY HIGH IONS NEAR ZERO VELOCITY

3.1. *Column Densities*

High ion species included in this study are N V and C IV. The N V λ1238.821 absorption line, with an equivalent width of 0.070 Å, has a formal statistical significance of 3.9 σ (Table 1).

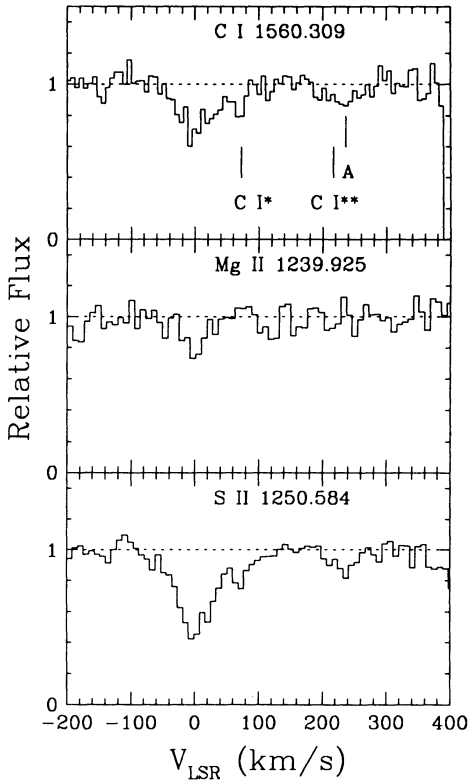

FIG. 3.—Comparison of relative velocity scale of our spectrum shown in Fig. 1 with that of the spectrum obtained by Maran et al. (1994) which contains the C IV λλ1548.195, 1550.770 and the C I λ1560.309 absorption used in this study. The fact that the velocity of the strongest part of absorption in C I is consistent with that of the Mg II and S II absorption (which occur in our spectrum shown in Fig. 1) suggests that there is no significant relative velocity shift between the two spectra. The expected positions of C I* λ1560.682 and C I** λ1561.438 absorption from the zero velocity gas are marked. The absorption feature labeled "A" is most likely due to C I λ1560.309 absorption from the HVC at $v_{LSR} = +240$ km s^{-1}, with possibly a small contribution from C I** λ1561.438 associated with the zero velocity gas.

The equivalent width of the weaker N V λ1242.804 line is consistent with both N V absorption lines being unsaturated. Assuming this, the equivalent width of the better-measured N V λ1238.821 line of the doublet implies a N V column density of $\log N(\mathrm{N\ V}) = 13.55 \pm 0.12$.

The C IV doublet lines are well observed. The upper two panels of Figure 4 show the distributions of *apparent* column density per unit velocity, $N_a(v)$, for both members. For a given absorption line, the apparent column density profile can be constructed according to

$$N_a(v)[\text{atoms cm}^{-2}\ (\text{km s}^{-1})^{-1}] = \left(\frac{m_e c}{\pi e^2}\right)\frac{\tau_a(v)}{\lambda f} = 3.768 \times 10^{14}\,\frac{\tau_a(v)}{\lambda f}\,, \quad (1)$$

where f is the oscillator strength of the line, λ is the wavelength of the line in Å, and $\tau_a(v)$ is the apparent optical depth given by

$$\tau_a(v) = \ln\left[I_c(v)/I_o(v)\right]\,, \quad (2)$$

where $I_o(v)$ is the observed intensity at velocity v, and $I_c(v)$ is the estimated continuum intensity at the same velocity. The $N_a(v)$ distribution is the instrument-smeared version of the intrinsic distribution if the absorption line does not contain unresolved,

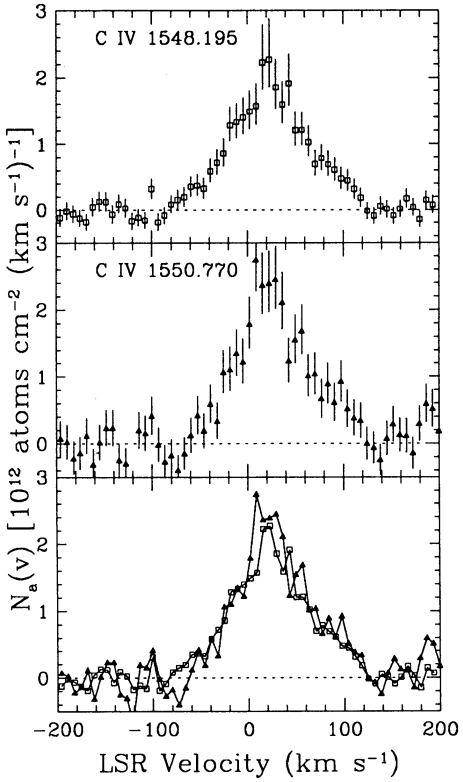

FIG. 4.—Distributions of apparent column density per unit velocity interval, $N_a(v)$, for the C IV doublets (*top two panels*). The bottom panel shows the comparison of the two $N_a(v)$ distributions.

saturated components. A complete discussion of the $N_a(v)$-technique may be found in Savage & Sembach (1991).

The bottom panel of Figure 4 shows the comparison of $N_a(v)$ for the C IV doublet members. The good match between the two distributions suggests that the C IV absorption lines do not contain substantial amounts of saturated, unresolved components, otherwise the distribution for the stronger member would fall *systematically* below that for the weaker member. Direct integrations of $N_a(v)$ in the velocity range $-80 < v_{LSR} < 120$ km s^{-1} yield log N(C IV) = 14.29 $\pm$ 0.04 for the stronger member, and log N(C IV) = 14.31 $\pm$ 0.05 for the weaker member. We adopt log N(C IV) = 14.30 $\pm$ 0.03 as the final result.

3.2. *Absorption Line Profiles*

Close inspection of the absorption profiles shown in Figure 2 reveals that the cores of C IV absorption are shifted by 20–30 km s^{-1} toward positive velocity relative to that of the S II absorption (the shift between the core of the Si II absorption and that of the S II absorption is due to a completely different reason; see § 4.1). The N V absorption lines show a similar shift relative to the S II lines. This systematic velocity shift between high and low ion lines is unlikely due to any relative shift in wavelength scales between the spectrum containing the S II absorption and that containing the C IV absorption (see § 2.4). Such a shift probably reflects the relative distributions of neutral and highly ionized gas in the Galaxy, as detailed below.

Studies of the H I gas distribution in the Galaxy (Lockman 1984) indicate that the neutral gas is distributed close to the Galactic disk, with a cold component having an exponential vertical scale height of $\sim$120 pc, and a warm component having a scale height of $\sim$500 pc. On the other hand, surveys for high ion absorption produced by Milky Way disk and halo gas (Savage & Massa 1987; Sembach & Savage 1992; Savage et al. 1993a) indicate that the highly ionized gas has a scale height of 3–5 kpc, with a midplane density of $\sim 10^{-9}$ to 10^{-8} cm^{-3}. The sight line toward NGC 3783 has a Galactic longitude $l = 287.46$ and latitude $b = +22.95$. At this relatively low latitude, Galactic rotation will have a significant effect on the absorption line profile if the gas distribution extends to large vertical distances. Figure 5 shows the relationship between the expected LSR velocity and the z distance (or distance from the Sun d) for gas participating in Galactic rotation in the direction of NGC 3783. It is clear that the core of S II absorption, which is produced mostly by the neutral gas in the disk (small z distance), should appear at a lower LSR velocity than that of the C IV absorption, for which the extended gas distribution in the z direction means that there will be significant C IV absorption at large positive velocities.

The well-observed C IV profiles toward NGC 3783 and the relatively low latitude of the direction makes the sightline suitable for a *quantitative* study of the effect of Galactic rotation on the high ion line profiles. This is an independent approach from the usual practice of modeling the N(C IV)$|\sin b|$ vs. $|z|$ distribution for a large sample of sight lines (see Sembach & Savage 1992). To model the profile, we assume that highly ionized gas follows an exponential distribution in the z direction with an exponential scale height h, midplane density n_0, and Doppler parameter b. We further assume that the gas at large z corotates with the underlying disk. Motions of the gas in the z direction should not appreciably affect the observed profile because the low latitude of the sight line reduces the projected component of those motions to $0.39v_z$. With these assumptions we can generate absorption line profiles for different adopted model parameters and compare them with the

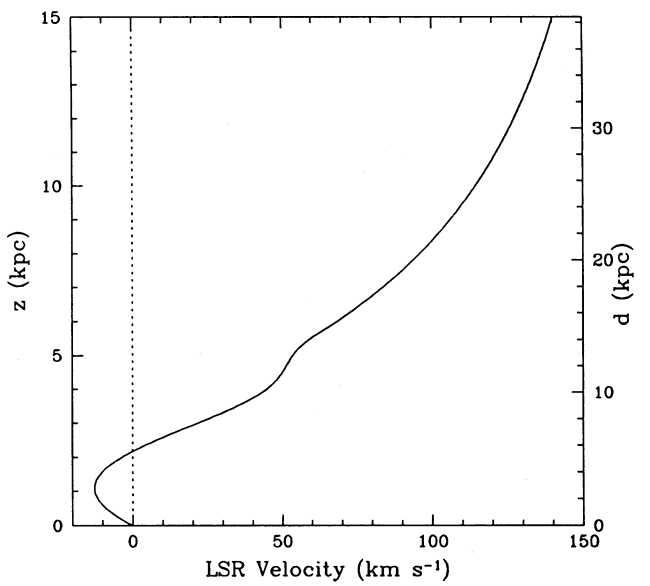

FIG. 5.—Expected relationship between line-of-sight LSR velocity and vertical distance from the Galactic plane (scale on the left) for gas clouds participating in Galactic rotation for the sight line toward NGC 3783. The corresponding distance from the Sun is indicated with the scale on the right. The bump near $v_{LSR} \sim +55$ km s^{-1} reflects a dip in the Galactic rotation curve (Clemens 1985).

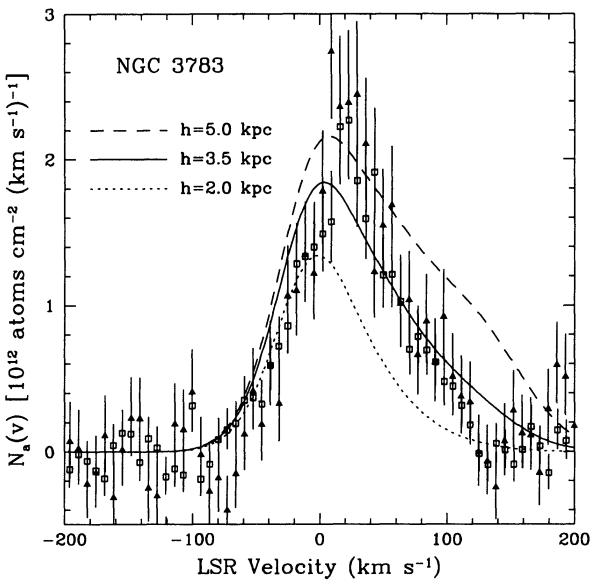

FIG. 6.—Corotation profile analyses for the C IV doublet toward NGC 3783. The C IV gas is assumed to have a simple exponential density distribution in the z direction. The open squares are the observed distribution for C IV λ1548.195, and the filled triangles are for C IV λ1550.770. Error bars are 1 σ. The smooth curves are model corotation profiles with midplane density $n_0 = 8.1 \times 10^{-9}$ cm^{-3}, Doppler $b = 34$ km s^{-1}, and exponential scale heights $h = 2$ kpc (*dotted curve*), 3.5 kpc (*solid curve*), and 5 kpc (*dashed curve*), with $h = 3.5$ kpc being the "best fit."

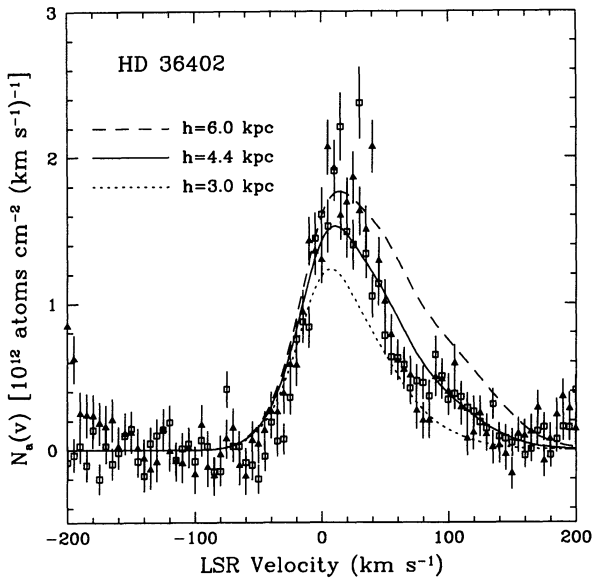

FIG. 7.—Similar to Fig. 6, but for the C IV doublet toward the star HD 36402 in the LMC. The observed distributions are from *IUE* data (Sembach & Savage 1992). The three model profiles are for midplane density $n_0 = 6.1 \times 10^{-9}$ cm^{-3}, Doppler $b = 24$ km s^{-1}, and exponential scale heights $h = 3$ kpc (*dotted curve*), 4.4 kpc (*solid curve*), and 6 kpc (*dashed curve*), with $h = 4.4$ kpc being the "best fit."

observed line profiles after convolution with the instrumental line spread function (see Sembach, Savage, & Massa 1991). We adopt the Galactic rotation curve from Clemens (1985), where the rotation velocity in the solar neighborhood is 220 km s^{-1}, and the Sun is at a Galactocentric distance of 8.5 kpc. The results of this exercise are shown in Figure 6, where the best fit as determined from χ^2 minimization yields the parameters $h = 3.5$ kpc, $n_0 = 8.1 \times 10^{-9}$ cm^{-3}, and Doppler $b = 34$ km s^{-1}. This scale height is similar to previous values obtained with the $N|\sin b|$ vs. $|z|$ method (Sembach & Savage 1992; Savage et al. 1993a). Also shown in Figure 6 are the corotation profiles for two different scale heights: $h = 2$ and 5 kpc.

We note that while the positive velocity extension of the C IV absorption profiles can be roughly explained with the simple exponential plus corotation model described above, the details do not match. In particular, the simple exponential plus corotation model cannot match both the *position* and *strength* of the peak of the C IV absorption *simultaneously*. We obtained a reduced χ^2 of 2.12 for the best fit.[5]

To see if the above mismatches are specific to the NGC 3783 sight line, we carried out a similar analysis for the C IV absorption toward the LMC star HD 36402 obtained with the *IUE* (Sembach & Savage 1992). The C IV profiles were obtained by summing up multiple exposures of *IUE* spectra, and they represent some of the best measured profiles toward extragalactic objects with the *IUE* satellite. The HD 36402 sight line is also particularly relevant since it has a similar Galactic longitude as the NGC 3783 sight line, but is on the *opposite* side of the Galactic disk (HD 36402 has $l = 277.8$ and $b = -33.0$, while NGC 3783 has $l = 287.46$ and $b = +22.95$). The results are shown in Figure 7, where the best-fit model has a scale height $h = 4.4$ kpc, midplane density $n_0 = 6.1 \times 10^{-9}$ cm^{-3}, and Doppler $b = 24$ km s^{-1}, with a reduced χ^2 value of 2.49.[6]

Comparing Figures 6 and 7 it is clear that the two sightlines show similar characteristics, and the corotation model with simple exponential gas distribution only provides a rough approximation to the actual profiles.

3.3. *Discussion*

There are several possible explanations for the mismatch between the observed absorption profiles and that calculated for the simple corotating model with an exponential gas distribution.

One possibility is that the assumption that the C IV gas distribution in the z direction can be represented by an exponential function is invalid. For this reason, we decided to revisit a model proposed by Spitzer (1956) in which hot halo gas is approximated by an isothermal, plane-parallel distribution that is in hydrostatic equilibrium with the gravity of the Galaxy. Adopting the empirical results of Kuijken & Gilmore (1989a, b) for the gravitational field of the Galaxy appropriate for the solar neighborhood, we have from equations (3) and (4) of Spitzer (1956):

$$n(z) = n_0 e^{-[93.1(\sqrt{z^2+180^2}-180)+0.0214z^2]/T}, \quad (3)$$

where n_0 is the midplane density, T is the isothermal gas temperature, and z is the vertical distance in parsecs. Replacing the exponential gas distribution in the corotation model with equation (3), we find the following best-fit parameters: temperature $T = 8.2 \times 10^5$ K, midplane density $N_0 = 6.2 \times 10^{-9}$

[5] The quoted χ^2 value is for the velocity range $[-80, +120]$ km s^{-1}, where significant C IV absorption occurs. For the velocity range $[-300, +300]$ km s^{-1}, within which the model fitting was performed, the reduced χ^2 value is 1.25.

[6] The quoted χ^2 value if for the velocity range $[-80, +120]$ km s^{-1}, where significant C IV absorption occurs. For the velocity range $[-200, +200]$ km s^{-1}, within which the model fitting was performed, the reduced χ^2 value is 2.19.

cm^{-3}, and Doppler $b = 34$ km s^{-1} (thermal width for the quoted temperature). It is interesting that the best-fit temperature is consistent with that required to explain the ionization of the gas. However, the fit of the isothermal/hydrostatic plus corotation model to the observed C IV profiles toward NGC 3783 (yielding a reduced $\chi^2 = 1.78$ for the velocity range $[-80, +120]$ km s^{-1}) is not significantly better than the exponential gas distribution. We also considered a Gaussian distribution of $n(z)$ in place of the exponential gas distribution and found that it did not improve the fit to the observed profiles.

Another possibility is that while the distribution of highly ionized gas in the z direction can roughly be described by a simple exponential function, there are sight-line pecularities. This is not surprising since the $N|\sin b|$ vs. $|z|$ distribution for C IV exhibits a large scattering (peak-to-peak scattering of roughly a factor of 10; see Sembach & Savage 1992). The mismatch between the simple exponential plus corotation model and the observations could be due to an enhancement in the C IV gas density at a $v_{LSR} \sim +20$ km s^{-1} ($z \sim 3$ kpc for corotating gas). This enhancement could be the result of a spiral arm (there is indeed a spiral arm at the longitudes of NGC 3783/HD 36402 at about the right velocity; see Figs. 3 and 4 of Davies 1972), or high-z gas photoionized by extragalactic photons. Note that the latter hypothesis is not in direct contradiction with the known results that the observed properties of highly ionized inner halo gas are generally better matched by models involving collisional ionization rather than photoionization (see discussion later in this subsection). Previous observations with the *IUE* generally have not probed large enough z distances to reveal a possible photoionized gas layer at $z > 3$ kpc.

Despite of the imperfect match between the models and the observed C IV profiles, the simple fact that the C IV profiles toward both NGC 3783 and HD 36402 can be *roughly* described by a corotation model plus exponential gas distributions with scale heights of 3–4 kpc indicates that large amounts of C IV–producing gas exist at $z > 3$ kpc along the NGC 3783 and HD 36402 sight lines. There has been some criticism in the past that determinations of high ion scale heights (see Sembach & Savage 1992) were probably biased by the few extragalactic data points, which almost exclusively refer to the measurements toward objects in the LMC and the SMC. In particular, York (1988) pointed out that the strong high ion absorption (therefore large column densities) toward the LMC and the SMC sight lines may be due to ionized gas associated with the LMC and the SMC instead of the halo of the Milky Way. The existence of large amounts of C IV gas toward NGC 3783 with $z > 3$ kpc argues against York's interpretation since the NGC 3783 sight line has a similar Galactic longitude as the Magellanic Clouds, but is on the *opposite* side of the Galactic plane. On the other hand, the lack of significant C IV absorption at velocities much beyond 100 km s^{-1} suggests that corotating highly ionized gas does not exist in substantial quantity at very large z distances ($z > 10$ kpc) along the NGC 3783 direction.

The N V absorption toward NGC 3783 is not observed well enough to allow for a meaningful profile analysis. However, we note that the *range* and the *center* of the N V absorption (especially the better-observed stronger member of the doublet) are very close to those of the C IV absorption (see Fig. 2), suggesting that the gas producing the N V absorption probably has a distribution similar to the gas that produces the C IV absorption. The N V ion is the most important hot gas diagnostic accessible with the *HST* because of the large amount of energy (77 eV) required for its creation. In comparison, Si IV and C IV, the two other hot gas diagnostics accessible with the *HST*, take 33 and 47 eV to create, respectively. Under conditions of collisional ionization equilibrium, the Si IV, C IV, and N V ions peak in abundance at temperatures approximately 6×10^4, 1×10^5, and 2×10^5 K, respectively (Sutherland & Dopita 1993). As such, the detection of N V gas in the Galactic halo generally indicates the presence of hot gas instead of photoionized gas because it is very difficult to produce N V with radiation from hot stars, given the expected presence of strong He^+ edge absorption at 54 eV in the stellar atmosphere. Previous studies suggest that photoionization-type models (Hartquist, Pettini, & Tallant 1984; Chevalier & Fransson 1984; Hartquist & Morfill 1986; Bloemen 1987) generally produce too little N V gas to match observations, while Galactic fountain-type models (Shapiro & Field 1976; Bregman 1980; Edgar & Chevalier 1986) which allow for the ionizing radiation produced by the cooling gas (Shapiro & Benjamin 1991) seem to be able to produce the amounts of observed Si IV, C IV, and N V gas (cf. Sembach & Savage 1992). The measured C IV and N V column densities toward NGC 3783 are consistent with the cooling hot Galactic fountain interpretations.

The C IV and N V column densities toward NGC 3783 are about half (or about a factor of 5 below if projected on the z direction) those along the well-studied 3C 273 sight line (Savage et al. 1993b). To date, all studies (Savage et al. 1993a; Burks et al. 1993) indicate that the 3C 273 sight line has the highest projected high ion column densities. This probably reflects the fact that the 3C 273 sight line penetrates through radio Loops I and IV, which are believed to be superbubbles created by past supernova events. The interiors of these superbubbles are probably too hot to contain appreciable C IV or N V gas, but the surrounding shells probably do contain these ions. It is interesting to note that even though both the projected C IV and N V column densities toward NGC 3783 are about a factor of 5 lower than that toward 3C 273, the ratio of C IV to N V, $N(\text{C IV})/N(\text{N V}) = 5.6 \pm 1.6$, is nearly identical to that along the 3C 273 sight line [$N(\text{C IV})/N(\text{N V}) = 5.9 \pm 1.6$] NGC 3783 and 3C 273 have nearly identical Galactic longitude (287.46 vs. 289.95). The NGC 3783 sight line also passes through radio Loop I, but not Loop IV. Thus, the similar ratios of $N(\text{C IV})/N(\text{N V})$ toward these two sight lines may point to the same ionization mechanism of the gas in the radio loops. In comparison, Sembach & Savage (1992) found an average ratio of $N(\text{C IV})/N(\text{N V}) = 4.6 \pm 2.7$ for a large sample of halo sight lines. Since supernova events are invoked in the galactic fountain models for creating the hot fountain gas in the first place, it is perhaps not too surprising that superbubbles like Loops I and IV may contain highly ionized gas whose properties resemble those predicted in the generic cooling fountain models.

4. ABSORPTION BY LOW IONS NEAR ZERO VELOCITY

4.1. *Velocities of Absorption*

In addition to the high ion species discussed in the previous section, the spectrum shown in Figure 1 also shows absorption by low ion species near zero velocity, including Mg II λ1239.925, S II $\lambda\lambda$1250.584, 1253.811, 1259.519, and Si II λ1260.422.

The profiles of the three S II absorption lines are shown in Figure 2. The cores of the S II absorption occur roughly at the

velocity where the 21 cm emission peaks, as expected. Despite the poor resolution of the instrumental combination of medium resolution grating with the LSA, the intermediate 21 cm velocity feature at $v_{LSR} \sim +62$ km s^{-1} clearly shows up in all three S II lines. These lines apparently trace the bulk of neutral gas along the sight line. Similar velocity structures are seen in the Ca II absorption obtained by West et al. (1985), although with considerably more detail owing to the better resolution (FWHM = 18 km s^{-1}) of the optical data. In particular, West et al. (1985) identified Ca II components at $v_{LSR} \sim +40$ and $+64$ km s^{-1}, which agree quite well with the components seen in 21 cm emission at $v_{LSR} \sim +35$ and $+62$ km s^{-1}. The fact that the Ca II intermediate velocity absorption has similar structures to that of the 21 cm emission suggests that the 21 cm intermediate velocity profile is probably not too far from the true H I gas distribution along the line of sight subtended by NGC 3783, even though the 21 cm data were obtained with a large (FWHM = 21′) beam. This has important implications for the discussion in the next section.

The Si II λ1260.422 line is one of the most sensitive tracers of neutral gas. The Si II absorption produced by the low ($v_{LSR} \sim -5$ km s^{-1}) and intermediate velocity ($v_{LSR} \sim +62$ km s^{-1}) gas is heavily saturated. Thus, no useful column density information is available for Si II. However, the enormous width of the Si II absorption, covering the range $-90 < v_{LSR} < +340$ km s^{-1} (including both the gas near zero velocities and the HVC at $v_{LSR} = +240$ km s^{-1}), is noteworthy in that low ion absorption lines of similar velocity spread are commonly found in the metal-line absorption systems in spectra of high-redshift quasars (see § 5.4 for more discussion).

4.2. *Metallicity of the Intermediate Velocity Cloud*

The S II absorption lines are especially useful since S is generally not depleted in the interstellar medium (ISM). Thus, the abundance of S relative to H provides a good measure of metallicity of the gas without the complication of depletion of elements onto dust grains. In Figure 8 we show the distributions of apparent column density per unit velocity, $N_a(v)$, for the three S II lines. The fact that the value of $N_a(v)$ for the stronger S II lines consistently lies below that for the weaker ones in the velocity range $-30 < v_{LSR} < +30$ km s^{-1} suggests that the S II lines contain saturated, unresolved absorption components in the core of the absorption [thus a direct integration of $N_a(v)$ over the above velocity range would underestimate the true column density]. This is not surprising given the strong 21 cm emission and the narrow width of the components in that velocity range. In contrast, the distributions of $N_a(v)$ beyond the core of S II absorption are consistent with each other to within the errors, indicating that part of the absorption does not contain saturated, unresolved components.

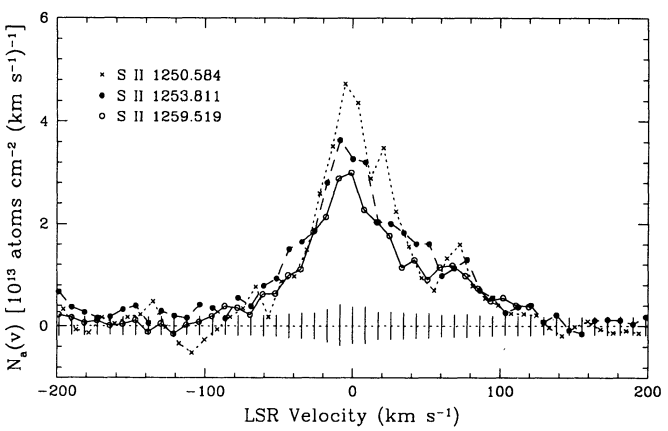

FIG. 8.—Distributions of apparent column density, $N_a(v)$, for the S II triplet absorption lines near zero velocity. The vertical bars at the bottom show the $\pm 1\,\sigma$ uncertainties appropriate for the S II λ1253.811 line (the uncertainties for the other two lines are similar). The distributions show evidence of saturated, unresolved components in the core ($-30 < v_{LSR} < +30$ km s^{-1}), but are consistent with no saturated, unresolved components away from the core.

Given the fact that the Ca II absorption shows similar velocity structures in the intermediate velocity gas as that of the 21 cm emission (§ 4.1), it is likely that the 21 cm intermediate velocity profile is close to the true line-of-sight H I distribution. Thus a determination of metallicity for the intermediate velocity gas through N(S II)/N(H I) may not be significantly affected by the differences in sampling geometries between the UV data (pencil beam, referring to a infinitesimally small solid angle) and the 21 cm radio data (obtained with a 21′ beam). Such a statement cannot be made for the lower velocity gas because the Ca II absorption shows very different velocity structures from that of the 21 cm emission at $v_{LSR} < +20$ km s^{-1}. For example, the Ca II absorption (West et al. 1985) clearly shows components at $v_{LSR} \sim -39$ and -1 km s^{-1}. While the $v_{LSR} \sim -1$ km s^{-1} Ca II component may correspond to the 21 cm components near -2 and -8 km s^{-1} (which would be blended at the resolution of the Ca II data), no distinct component corresponding to the -39 km s^{-1} Ca II feature is present in the 21 cm emission. This suggests that there may be substantial difference in the line-of-sight H I distribution toward NGC 3783 with that obtained with radio telescope with a 21′ beam width for the low-velocity gas.[7]

Since there is some blending between the intermediate velocity feature at $v_{LSR} \sim +62$ km s^{-1} with the lower velocity component at $v_{LSR} \sim -5$ km s^{-1} in 21 cm, and since the blending is much worse in the S II lines due to the broad line spread function, the usual practice of estimating H I and S II column densities by directly integrating the $N_a(v)$ distributions in a specified velocity range is not applicable, even if no unresolved, saturated components are present. We thus take the following approach.

If we make the assumption that the 21 cm emission profile observed with the 21′ beam is close to the line-of-sight H I distribution (which is more likely true for the intermediate velocity gas than for the low-velocity gas as discussed above), we can convert the distribution of column density per unit velocity interval for H I into that of S II by adopting some S abundance and assuming that N(S II)/N(H I) = N(S)/N(H). The resulting $N_a(v)$ for S II can be easily converted into optical depth per unit velocity interval to create a model S II absorption line profile using equations (1) and (2). The model S II line profile can then be convolved with the instrumental line spread function and compared with the observed line profile. An estimate of the S abundance may be obtained by adjusting the

[7] The -39 km s^{-1} Ca II component has similar apparent optical depth as the $+40$ and $+64$ km s^{-1} Ca II components. Thus, one expects the 21 cm emission corresponding to the -39 km s^{-1} Ca II component to have similar strength as these corresponding to the $+40$ and $+64$ km s^{-1} Ca II components (assuming they all have similar chemical and physical conditions), which is not the case (Fig. 2, top right panel). Hence the lack of 21 cm emission component corresponding to the -39 km s^{-1} Ca II feature is probably not due to the lower sensitivity of the 21 cm data relative to the Ca II data.

input abundance to get a good match. Since the low-velocity gas at $v_{LSR} \sim -5$ km s^{-1} is likely to have solar metallicity, while the metallicity of the intermediate velocity gas is totally unknown, it is desirable that the two parts of absorption be modeled independently.

The actual modeling procedure is as follows: As an approximation, we assume that the gas in the velocity range $-60 < v_{LSR} < +20$ km s^{-1} has a metallicity independent of velocity. We first generate the expected S II line profile as described above for some assumed metallicity for the gas in the velocity range $-60 < v_{LSR} < +20$ km s^{-1}, and then convolve it with the line spread function shown in Figure 2. The resulting convolved line profile is compared to the observed line profile. The assumed metallicity is adjusted until a good match is found for the negative-velocity wing of the absorption, which should contain little contribution from the absorption by the intermediate velocity gas. The convolved model absorption profile is then divided into the observed profile to remove the absorption by the low-velocity gas, thus effectively re-creating the "continuum" over which the absorption by the intermediate velocity gas occurs. The above procedure is then repeated for the intermediate velocity gas defined as $+20 < v_{LSR} < +100$ km s^{-1}. Figure 9 shows the results of this modeling process for S II λ1253.811. Panel (*a*) shows the 21 cm profile from Danly et al. (1994; same as that shown in Fig. 2). Panel (*b*) shows the results of modeling the absorption by the low-velocity gas. The best match of profiles requires a S abundance for the low-velocity gas of 0.7 times the solar value. Note that this abundance is quite uncertain due to the extreme saturation of the absorption line at these velocities. The bottom three panels show the results of modeling the intermediate velocity absorption using S abundances of 0.5, 0.3, and 0.7 times solar values, representing respectively the "best" fit and the lower and upper limits. Note that the histogram in the bottom three panels is the observed line profile after removing the absorption by the low-velocity gas.

We would like to emphasize that the only purpose of modeling the low-velocity gas absorption is to estimate the effective "continuum" for the intermediate velocity gas absorption. Knowing that the S II absorption by the low-velocity gas is heavily saturated in the core, the S abundance used to model the low-velocity absorption is very uncertain. We found that any S abundance between 0.5 to 1 solar would give a reasonable fit to the S II line profile in the negative-velocity wing of the S II absorption. The fact that the low-velocity absorption is better explained by a S abundance of 0.7 times solar instead of solar (as might be expected) may by itself be an indication that the 21 cm emission profile recorded with a large beam (21′) by Danly et al. (1994) toward NGC 3783 does not represent the true line-of-sight gas distribution. Indeed, the emission-like feature near -30 km s^{-1} in the continuum-corrected spectrum (panels *c*, *d*, and *e* of Fig. 9) could be due to the -39 km s^{-1} absorption feature that is present in the Ca II absorption (and presumably also present in the S II absorption), but not accounted for in the 21 cm emission data. On the other hand, the absorption by the intermediate velocity gas is only lightly saturated (see discussion at the beginning of this subsection and the model profiles in Fig. 9 before convolution) so the S abundance thus determined should be reliable.

Modeling of the other two S II absorption line profiles yields consistent, but less certain results because the S II λ1250.584 line is considerably weaker than the S II λ1253.811 line, while the S II λ1259.519 absorption, through stronger, is severely

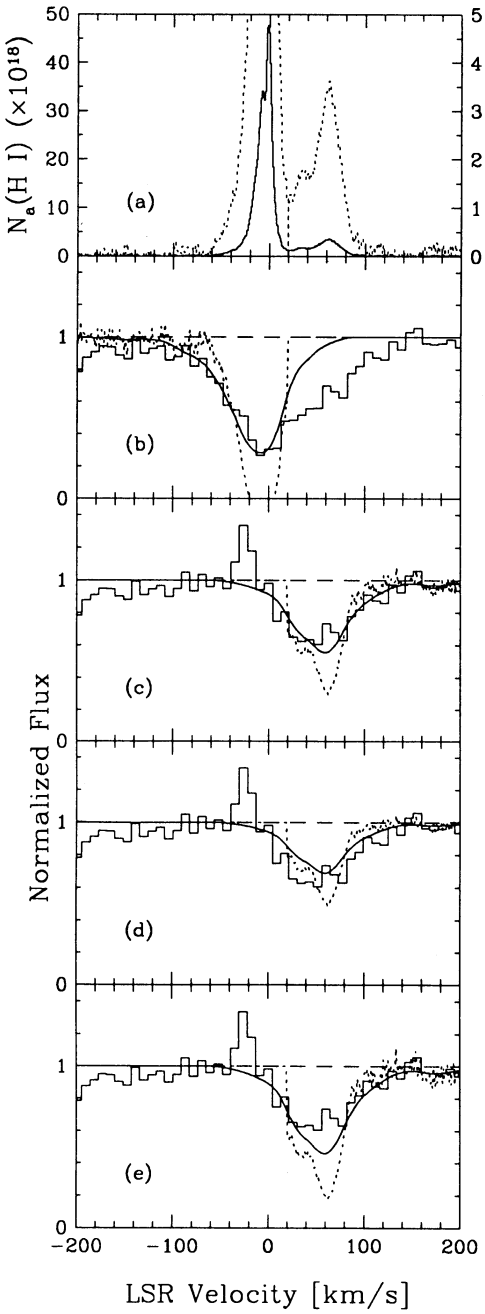

FIG. 9.—Estimate of S abundance for the intermediate velocity gas near $v_{LSR} \sim +62$ km s^{-1} using the S II λ1253.811 line. (*a*) 21 cm emission profile (*solid line*) in unit of 10^{18} atoms cm^{-2} [km s^{-1}]$^{-1}$ from Danly et al. (1994). The dotted line is the same profile expanded by a factor of 10 in vertical scale (appropriate for the scales on the right). (*b*) Modeling the low-velocity gas absorption. The dotted curve is the expected S II λ1253.811 profile for the gas distribution with $v_{LSR} < +20$ km s^{-1} assuming 0.7 times solar abundance for S. The solid smooth curve is the expected S II profile convolved with the line spread function. The solid histogram is the actual observed profile of S II λ1253.811. (*c*) Modeling the intermediate velocity gas absorption. The dotted curve is the expected S II λ1253.811 profile for the gas distribution with $v_{LSR} > +20$ km s^{-1} assuming 0.5 times solar abundance for S, and the solid line is the same profile convolved with the line spread function. The solid histogram is the observed S II λ1253.811 profile after removing the absorption by the low-velocity gas. (*d*) same as (*c*) but for S abundance of 0.3 times solar for the intermediate velocity gas. (*e*) same as (*c*) but for S abundance of 0.7 times solar for the intermediate velocity gas. The best-fit result for the intermediate velocity gas absorption is (*c*) with a S abundance of 0.5 times solar value.

blended with the neighboring Si II λ1260.422 line. Given the uncertainty in modeling the low-velocity gas absorption to reconstruct the effective "continuum" for the intermediate velocity absorption, we conservatively conclude that S/H = 0.5 ± 0.2 times the solar value for the intermediate velocity gas near $v_{LSR} \sim +62$ km s^{-1}. Note that the above error does not account for the possibility that the line-of-sight H I distribution for the intermediate velocity gas toward NGC 3783 may be quite different from the 21 cm emission used here, which was obtained with a large beam width (21′).

4.3. *Origin of the Intermediate Velocity Cloud*

Few estimates of metallicity for intermediate and high-velocity clouds exist in the literature. Using *IUE* observations of SN 1987A in the LMC, Blades et al. (1988) obtained estimates of metal abundances for the intermediate and high-velocity clouds at v_{LSR} = 70, 129, and 171 km s^{-1} toward that direction in order to determine whether these clouds originate from the Galaxy (halo) or from the LMC. They found that the 70 km s^{-1} cloud has approximately solar abundance, while the other two clouds have roughly 30% solar abundance. However, relatively reliable abundances were determined only for the elements of Mg, Al, Si, and Fe (and Cr, Mn, and Ni for the 70 km s^{-1} cloud alone). One of the problems with these estimates is that the elements being studied are all refractory elements, which are depleted onto dust grains easily. Given the lack of any knowledge of dust information in these clouds, it is not clear if the clouds have intrinsically a low metallicity, or if they have solar metallicity but with some of these elements depleted onto dust grains. Indeed, the recent study of intermediate velocity gas toward the halo star HD 93521 at z = 1.5 kpc by Spitzer & Fitzpatrick (1993) reveals that while S appears to have solar abundance in four clouds with velocity between −35 and −70 km s^{-1}, Ti, Fe, Mn, and Si are depleted by factors ranging from 8 to 2. Our estimate of the S abundance is important in that S is generally not depleted in the ISM, and thus the abundance obtained for the intermediate velocity gas, S/H = 0.5 ± 0.2 times solar value, probably represents its true metallicity. Of course all estimates of elemental abundances for intermediate and high-velocity clouds to date are subject to the same uncertainty in using H I column densities obtained with a large radio beam in place of the line-of-sight H I column density (see discussion in § 5.3 for possible ways of avoiding such a problem).

The likelihood that the intermediate velocity gas at $v_{LSR} \sim +62$ km s^{-1} has about half the solar metallicity is intriguing. It is well known that there is a metallicity gradient in the Galactic disk in that metallicity decreases with increasing galactocentric distance at a rate of about 0.08 dex per kpc (Shaver et al. 1983). Assuming that the intermediate velocity gas is a high-z extension of disk gas at large Galactocentric distances, and that it corotates with the disk, the velocity of the gas, $v_{LSR} \sim +62$ km s^{-1}, would put it at a line-of-sight distance of ∼14 kpc from the Sun, or about the same distance from the Galactic center (assuming the Sun is 8.5 kpc from the Galactic center). If the metallicity gradient relation holds for galactocentric distances as large as 14 kpc, it would imply a metallicity for the cloud of ∼0.44 dex below (or ∼36%) solar. It is interesting that we obtain a roughly similar value (∼50% solar). If indeed the intermediate velocity gas is associated with the flared-up disk or an outer spiral arm that corotates with the underlying disk, then the implied vertical height of the gas is $z \sim 5$ kpc.

5. ABSORPTION BY HIGH-VELOCITY GAS

5.1. *Column Densities and Metal Abundances*

Absorption produced by the HVC at $v_{LSR} = +240$ km s^{-1} toward NGC 3783 is clearly seen in the low ion lines of S II (the S II λ1259.519 line is masked out by the strong Si II λ1260.422 absorption near zero velocity) and Si II λ1260.422. Due to the complex instrumental smearing function, it is difficult to discern any velocity structures in the HVC absorption (but see the end of this subsection for the discussion of Si II λ1260.422 HVC absorption). In any case, the relatively symmetric absorption profiles of the S II absorption are consistent with the symmetric 21 cm HVC profile (West et al. 1985; see the reproduction in our Fig. 2). No C IV or N V absorption at the velocity of the HVC is detected. The corresponding 2 σ upper limits (assuming the lines are unresolved) are 0.07 Å [N(C IV) < 1.7 × 10^{13} cm^{-2}] for the C IV doublet lines, and 0.04 Å [N(N V) < 1.8 × 10^{13} cm^{-2}] for the N V doublet lines.

The relative strength of the two unblended S II HVC lines suggests that the S II HVC absorption lines are not saturated. The derived S II column density assuming the lines are on the linear part of curve of growth is then N(S II) = 3.4 × 10^{14} cm^{-2}. West et al. (1985) measured a total H I column density for this HVC of N(H I) = 1.21 × 10^{20} cm^{-2}. We thus find N(S II)/N(H I) = 2.8 × 10^{-6}. Adopting a solar S abundance of log (S/H)$_{\odot}$ + 12 = 7.27 (Anders & Grevesse 1989), the above ratio implies a S abundance of S/H = 0.15 ± 0.05 times the solar value for the HVC assuming that S II is the dominant ion stage of S in the HVC. The latter assumption is likely to be valid because S II has an ionization potential of 23.3 eV which is above the 13.6 eV required to ionize neutral hydrogen.

Given that S is usually undepleted in the diffuse interstellar medium, the above S abundance, S/H = 0.15 ± 0.05 times the solar value, likely represents the true metallicity of the HVC. The HVC has a relatively high total H I column density so that ionization corrections are likely to be small. The major uncertainty in the above abundance determination lies in the fact that the UV absorption samples the *line of sight* material toward NGC 3783, while the 21 cm observation was made with a 34′ beam (West et al. 1985 and Morras & Bajaja 1983). It is well known that HVCs show substantial small-scale ($\ll$1°) structures. For example, Wakker & Schwarz (1991) found that the H I column density of HVCs can vary by a factor of 5 over scales as small as 1′. Thus, the line of sight N(H I) toward NGC 3783 could be quite different from that measured from the 21 cm emission using a large beam width. Unfortunately, at $v_{LSR} = +240$ km s^{-1}, the Lyα absorption line from the HVC is so badly blended with that from the zero velocity gas that a determination of the line of sight N(H I) in the HVC from Lyα absorption is impossible.

While S is generally undepleted in the diffuse interstellar medium, Si usually is depleted by a factor of ∼10 (Jenkins 1987). Thus in principle the relative abundance of Si to S provides some information on the depletion, and thus on the dust grains that may be present in the HVC. Unfortunately the Si II λ1260.422 HVC absorption is badly blended with the zero-velocity absorption line of the same ion species. Given the strength of the absorption, the Si II λ1260.422 HVC absorption line is almost certainly saturated. Attempts to model the Si II HVC absorption profile with the 21 cm emission data using similar procedures as outlined in § 4.2 have failed to yield any definitive conclusions. This is partly because the HVC Si II absorption is heavily saturated in the core over a substantial

velocity range ($\Delta v > 50$ km s^{-1}) making the line profile insensitive to changes in the Si II column density, and partly due to the fact the Si II λ1260.422 transition is very sensitive to the distribution of low column density gas in the wings ($v_{LSR} < 220$ km s^{-1} and $v_{LSR} > 270$ km s^{-1}) of the 21 cm emission profile, which is not well determined owing to the limited S/N of the 21 cm data (see Fig. 4 of West et al. 1985). For example, the Si II λ1260.422 absorption line appears to have a component at $v_{LSR} \sim +190$ km s^{-1}, which is not present in either the 21 cm emission spectrum or the S II absorption lines. This component is most likely a very low column density cloud that is missed by the radio observation [which is sensitive to gas clouds with N(H I) > a couple times 10^{18} cm^{-2}], but picked up by the sensitive Si II λ1260.422 line. We estimate a strict lower limit of N(Si II) > 2.6×10^{13} cm^{-2} for the HVC by assuming that the absorption line is unsaturated. For a solar Si abundance of log $(\mathrm{Si/H})_\odot + 12 = 7.55$ (Anders & Grevesse 1989), the above column density implies Si/H > 0.006 times the solar value. This limit turns out to be not very useful.

5.2. *Physical Conditions in the High-Velocity Gas*

In this subsection, we will first argue that we have probably detected C I λ1560.309 absorption from the HVC at $v_{LSR} = +240$ km s^{-1}. We will then use this result to gain some information about the ionization conditions in the HVC.

We believe that the absorption feature labeled "A" in the top panel of Figure 3 (hereafter "Feature A") is mostly due to C I λ1560.309 absorption associated with the HVC at $v_{LSR} = +240$ km s^{-1}. Feature A occurs at a LSR velocity of +236 km s^{-1} in the velocity frame of C I λ1560.309 absorption associated with the zero velocity gas (top panel of Fig. 3). While this velocity is close to the separation between C I λ1560.309 and C I** λ1561.438 (separation $\Delta v = 217$ km s^{-1}) implying that Feature A could be C I** λ1561.438 absorption associated with the zero velocity gas, it is much closer to the velocity of the HVC at $v_{LSR} = +240$ km s^{-1}, suggesting that Feature A is more likely C I λ1560.309 absorption arising from the HVC. The relative strengths of the C I λ1560.309 and C I* λ1560.682 absorption from the zero velocity gas, and that of Feature A argues strongly for Feature A to be mostly due to C I λ1560.309 absorption from the HVC (see Jenkins & Shaya 1979).

The likely detection of C I absorption from the HVC is significant. As far as we know, this is the first time C I absorption has been seen in a HVC. Assuming our identification is correct, we estimate a column density of N(C I) $\sim 1.8 \times 10^{13}$ cm^{-2} from the equivalent width of Feature A assuming the line is unsaturated. It is surprising that the ratio of N(C I)/N(H I) $\sim 1.5 \times 10^{-7}$ is similar to that found in the local interstellar clouds with similar hydrogen column densities (Jenkins & Shaya 1979) on the assumption that the molecular fraction of hydrogen in the HVC is negligible.

The value of S/H ~ 0.15 times the solar value for the HVC at $v_{LSR} = +240$ km s^{-1} implies an even lower C abundance in the HVC because C/H is expected to be smaller than S/H based on the empirical abundance studies reviewed by Wheeler, Sneden, & Truran (1989). Since local interstellar clouds are expected to have solar metallicity, and since typical C depletion by dust is no more than $\frac{2}{3}$ (Cardelli et al. 1993), the HVC toward NGC 3783 is expected to have a lower *gas phase* C abundance than the local interstellar clouds. If C is depleted onto dust in the HVC, the gas phase abundance of C in the HVC would be expected to be even lower. Since the ratio of N(C I)/N(H I) in the HVC is similar to those in the local interstellar clouds with similar hydrogen column densities, it appears that the HVC toward NGC 3783 is more neutral (i.e., less ionized) than the local interstellar clouds on average. This could be due to either a lower ionizing photon density or a higher gas density in the HVC. Given the limited information available, a more quantitative analysis is not justified. Future higher quality data of similar nature should yield important new results regarding HVCs.

5.3. *Origin of the High-Velocity Gas*

Several decades after the discovery of HVCs, we still have little knowledge regarding their nature and origin (see Wakker 1991 for a review). Key factors that will help resolve these issues include determining locations of HVCs relative to the Galaxy, elemental abundances, and kinematical and physical conditions in these HVCs. From a study of Ca II absorption produced by HVC 287.5+22.5+240 toward NGC 3783, West et al. (1985) have argued that this HVC is most likely an extragalactic object whose gas is stripped away by tidal interaction with the Milky Way, although they could not rule out the possibility that the HVC is part of the Magellanic Stream. However, elemental abundance arguments based on Ca suffer the serious uncertainties that Ca can be easily depleted by dust grains. Thus there is no information as to whether the Ca abundance refers to the true metallicity of the gas, or is further modified by dust. In addition, Ca II is not the dominant ion stage of Ca in neutral gas, and differences in ionization conditions in the clouds will also affect the Ca II column densities. Our determination of the S abundance above is not subject to the same uncertainties. With the aid of the new information obtained in this study, we reconsider the issue of the origin of HVC 287.5+22.5+240. To assist the discussion, we note that the velocity of the HVC relative to the center of the Galaxy (i.e., Galactocentric velocity) is $v_{GSR} = v_{LSR} + 220 \sin l \cos b = +47$ km s^{-1}.

It has been suggested that intermediate and high-velocity clouds could be local gas accelerated to high velocity by supernova explosions (Spitzer 1976; de Noyer et al. 1977). However, such an explanation probably does not hold for HVC 287.5+22.5+240 because local gas is expected to have solar metallicity, which is incompatible with the low S abundance we find for the HVC. A related phenomenon to the supernova-accelerated gas is the Galactic fountain (Shapiro & Field 1976; Bregman 1980). The difficulty with this interpretation for the origin of HVC 287.5+22.5+240 is that low ions (such as C I, Si II, and S II) are not expected to be present in the fountain gas until the returning stage of the fountain gas to the disk, when the fountain gas has cooled and condensed. One expects the returning fountain gas to have negative Galactocentric velocities, contrary to $v_{GSR} = +47$ km s^{-1} for HVC 287.5+22.5+240. Another popular idea for the origin of intermediate and high-velocity clouds is that they are the high-z extensions of outer spiral arms (Kepner 1970; Davies 1972; Wannier, Wrixon, & Wilson 1972; Verschuur 1973). The low S abundance we find for the HVC seems to be qualitatively consistent with this interpretation since gas at large Galactocentric distances is expected to have relatively low metallicity. However, the large positive velocity of the HVC ($v_{LSR} = +240$ km s^{-1}) would put the gas at a Galactocentric distance of greater than 50 kpc if the gas roughly corotates with the underlying disk. It may then become difficult to interpret the *physical association* of the HVC with the Galaxy.

Mathewson et al. (1974) and Mathewson, Schwarz, & Murray (1977) proposed that HVC 287.5+22.5+240 is part of the Magellanic Stream being produced by tidal interactions between our Galaxy and the Magellanic Clouds. The argument is based on two facts. First, HVC 287.5+22.5+240 is at the tip of a HVC complex which, projected on the sky, appears to originate from the Magellanic Clouds, but is on the opposite side from the Magellanic Stream with respect to the Magellanic Clouds (see Figs. 2 and 3 of Mathewson et al. 1974). Second, the velocity of the HVC complex roughly agrees with that of the Stream. Analyses of stellar spectra by Russell & Bessell (1989), show that the LMC and the SMC have metallicities of Fe/H $\sim$ 0.5 and 0.2 times the solar value, respectively. However, these values may not be readily comparable with the value of S/H $\sim$ 0.15 times the solar value that we find for the HVC. Studies in the Galaxy show that at metallicities of Fe/H less than one-tenth of the solar value, the group of alpha elements, including Na, Mg, Al, Si, S, K, Ca, and perhaps Ti, is overabundant relative to Fe by about a factor of 2.5 (see Wheeler et al. 1989). If the same relation applies to the HVC, then the HVC should have an intrinsic Fe/H $\sim$ 0.06 times the solar value. This metallicity is significantly lower than that for the Magellanic Clouds. Another obvious difference between the HVC and the Magellanic Stream is that the HVC shows two-component structures in both the angular distribution (small concentrations buried in more diffuse extended envelopes) and the velocity profiles (narrow components with half-width <10 km s^{-1} on top of broader components with half-width $\sim$20–30 km s^{-1}). Such structures, while typical of high *negative* velocity clouds, are not seen in the Magellanic Stream clouds (Mathewson et al. 1974; Mirabel, Cohen, & Davies 1979; McKee, Newton, & Morton 1983). However, as noted by West et al. (1985), the differences in the angular distribution and velocity profiles could be due to differences in the physical conditions of the gas, such as temperature, density, etc. Given the uncertainty in the H I column density of the HVC for the determination of the S abundance, one cannot rule out the possibility that the HVC actually has the same metal abundance as the Magellanic Clouds. Thus a Magellanic Stream interpretation for the HVC remains viable.

Lynden-Bell (1976) suggested that some of the most prominent northern hemisphere complexes of high-velocity clouds are, like the Magellenic Stream, extragalactic objects in the Local Group that are in the process of interaction with the Galaxy. West et al. (1985) concluded that this is an attractive alternative for the origin of HVC 287.5+22.5+240 based on kinematical and abundance (for Ca) arguments. Our estimate of the low S abundance for the HVC is certainly consistent with this interpretation.

Although our conclusions regarding the origin of HVC 287.5+22.5+240 are not too different from those of West et al. (1985), we emphasize that our arguments put these conclusions on sounder ground. At the present, we cannot say for sure which of the last two possibilities above is correct. However, it is possible to resolve the issue with future observations. One of the uncertainties in the metal abundance determination is in the H I column density resulting from the differing sampling geometries. One way to avoid this uncertainty is to study the *relative abundance pattern* in the HVC. For example, if indeed S/H $\sim$ 0.15 times the solar value for the HVC, then one expects Zn/S $\sim$ 0.4 times the solar value, and O/S $\sim$ the solar value for the HVC, if the empirical relative abundance patterns found in the Galaxy apply in the HVC (see Wheeler et al. 1989). Since O, S, and Zn are all relatively unaffected by dust grains, the ratios should not be significantly biased by depletions. The relative abundance pattern for the HVC may be compared with that found in the Magellanic Stream clouds, which will then allow for a discrimination between the last two scenarios discussed above.

5.4. *Implications for Quasar Absorption Line Studies*

Regardless whether HVC 287.5+22.5+240 is associated with the Magellanic Stream or is another independent extragalactic object in the Local Group, the detection of significant metallicity in the cloud has important implications for understanding quasar absorption systems at high redshifts. It has been argued that the number density of metal absorption systems at high redshifts is so high that, if they are produced in the halos of spiral galaxies, these halos must have radial extent of $\geq$50 kpc (cf. Bergeron 1988). York and collaborators (York et al. 1986; York 1988; Yanny & York 1992) have argued that such large halos have not been detected observationally in the local universe, and they favor an interpretation of clustered gas-rich dwarf galaxies for the sites of these high-redshift absorption systems (the number density of dwarf galaxies in this picture has to be extremely high in order to explain the frequency of metal systems). The large velocity spread of absorption toward NGC 3783 ($>$300 km s^{-1} for Si II λ1260.422, including the HVC) indicates that complex absorption systems like those commonly seen in quasar metal-line systems can be produced in or near our Galaxy. If galaxy interactions are more common at high redshifts, the large number density of metal-line systems seen in our quasar spectra can be explained.

6. SUMMARY

We have obtained GHRS medium resolution observations of the bright Seyfert galaxy NGC 3783 in order to study the absorption produced by disk and halo gas in the Milky Way. The analysis of the data is supplemented by the observations of C IV $\lambda\lambda$1548.195, 1550.770 toward the same object, kindly made available to us by Maran et al. (1994). Our main results are as follows:

1. We detect absorption by Galactic disk and halo gas near zero velocity in C IV $\lambda\lambda$1548.195, 1550.770, N V $\lambda\lambda$1238.821, 1242.804, Si II λ1260.422, and S II $\lambda\lambda$1250.584, 1253.811, 1259.519. Absorption from disk gas is also detected in C I λ1560.309, C I* λ1560.682, C I** λ1561.438, and Mg II λ1239.309.

2. We also detect absorption by the high-velocity cloud HVC 287.5+22.5+240 at $v_{\rm LSR} = +240$ km s^{-1} in S II, Si II, and probably C I. No C IV or N V high-velocity counterparts are detected down to equivalent width limits (2 σ) of 0.07 Å [N(C IV) $< 1.7 \times 10^{13}$ cm^{-2}] and 0.04 Å [N(N V) $< 1.8 \times 10^{13}$ cm^{-2}], respectively.

3. The integrated C IV and N V column densities from zero velocity gas toward NGC 3783 are typical of other extragalactic sightlines. The detection of significant N V absorption toward NGC 3783 is consistent with the absorption being produced in the gas of a galactic fountain cooling from $T > 2 \times 10^5$ K.

4. The C IV absorption profiles toward NGC 3783 exhibit an asymmetric extension to large positive velocity similar to the effect previously found for absorption toward the LMC (Savage & de Boer 1979, 1981). Kinematic modeling reveals that the C IV profiles for NGC 3783 and a LMC sight line (HD

36402) are roughly described by corotating halo gas having exponential scale heights of 3.5 and 4.4 kpc, respectively. These kinematically derived scale heights are consistent with those obtained from plots of $N \mid \sin b \mid$ vs. $\mid z \mid$ for disk and halo stars.

5. We estimate an approximate S abundance, S/H = 0.5 ± 0.2 times solar, for the intermediate velocity gas at $v_{LSR} \sim +62$ km s^{-1} toward NGC 3783. The abundance measurement may be influenced by differences in sampling geometry as it relies on a H I column density based on 21 cm data obtained with a 21′ beam. The S abundance is consistent with that expected from the known metallicity gradient in the Galactic disk if the intermediate velocity gas is a corotating high-z extension of an outer spiral arm of the Galaxy at a Galactocentric distance of $\sim$14 kpc. If the interpretation is correct, the implied vertical height of the gas is $\sim$5 kpc above the disk.

6. The S II absorption lines associated with the HVC at $v_{LSR} = +240$ km s^{-1} result in a S abundance relative to the Sun of S/H = 0.15 ± 0.05 for the HVC. This constitutes the first reported measurement of S abundance in a HVC. This is significant because metallicity measurements based on S are generally free of uncertainties resulting from dust depletion effects. However, this estimate may be affected by differences in sampling geometry since the H I column density was estimated from 21 cm emission spectrum obtained with a 34′ beam width. The Si II HVC absorption is saturated, and no reliable column density for Si II can be deduced. The available evidence favors the Magellanic Stream or an independent extragalactic object in the Local Group interacting with the Galaxy as the likely origin for the HVC. This local Galactic absorption phenomena may have significant implications for the origin of quasar metal absorption line systems.

The observations discussed here would not have been possible without the dedicated effort of those people associated with the *HST* and GHRS projects. In particular, we would like to thank Derck Massa for providing a preliminary version of the code used to construct the corotation profiles, the late Marco Oliveri at the Space Telescope Science Institute for assisting the phase 2 preparation, and Jennifer Sandoval at the Goddard Space Flight Center for assisting the data handling. Helpful suggestions from an anonymous referee are appreciated. Support for this work was provided by NASA through grant numbers GO-3463.01-91A and HF1038.01-92A (for K. R. S.) from the Space Telescope Science Institute, which is operated by the Association of Universities for Research in Astronomy, Inc., for NASA under contract NAS 5-26555.

REFERENCES

Anders, E., & Grevesse, N. 1989, Geochim. Cosmochim. Acta, 53, 197
Bergeron, J. 1988, in QSO Absorption Lines: Probing the Universe, ed. J. C. Blades, D. A. Turnshek, & C. A. Norman (Cambridge: Cambridge Univ. Press), 127
Blades, J. C., Wheatley, J. M., Panagia, N., Grewing, M., Pettini, M., & Wamsteker, W. 1988, ApJ, 232, L75
Bloemen, J. B. G. M. 1987, ApJ, 322, 694
Bregman, J. N. 1980, ApJ, 236, 577
Burks, G. S., et al. 1993, ApJ, submitted
Burks, G. S., York, D. G., Blades, J. C., Bohlin, R. C., & Wamsteker, W. 1991, ApJ, 381, 55
Cardelli, J. A., Mathis, J. S., Ebbets, D. C., & Savage, B. D. 1993, ApJ, 402, L17
Chevalier, R. A., & Fransson, C. 1984, ApJ, 279, L43
Clemens, D. P. 1985, ApJ, 295, 422
Danly, L., Lockman, F. J., & Savage, B. D. 1994, in preparation
Davies, R. D. 1972, MNRAS, 160, 381
de Noyer, L. K., Button, L., Chaffin, D., & Nieznanski, J. 1977, ApJ, 213, 379
Duncan, D. K. 1992, Goddard High Resolution Spectrograph Handbook, version 3.0 (Baltimore: STScI)
Edgar, R. J., & Chevalier, R. A. 1986, ApJ, 310, L27
Fitzpatrick, E. L., & Savage, B. D. 1983, ApJ, 267, 93
Jenkins, E. B. 1987, in Interstellar Processes, ed. D. J. Hollenbach, & H. A. Thronson, Jr. (Dordrecht: Reidel), 533
Jenkins, E. B., & Shaya, E. J. 1979, ApJ, 231, 55
Hartquist, T. W., & Morfill, G. E. 1986, ApJ, 311, 518
Hartquist, T. W., Pettini, M., & Tallant, A. 1984, ApJ, 276, 519
Hulsbosch, A. N. M. 1975, A&A, 40, 1
Kepner, M. 1970, A&A, 5, 44
Kuijken, K., & Gilmore, G. 1989a, MNRAS, 239, 571
———. 1989b, MNRAS, 239, 605
Lockman, F. J. 1984, ApJ, 283, 90
Lockman, F. J., Jahoda, K., & McCammon, D. 1986, ApJ, 302, 432
Lynden-Bell, D. 1976, MNRAS, 174, 695
Maran, S. P., Reichert, G. A., Mushotzsky, R., Smith, A. M., Carpenter, K. S., Hutchings, J. B., & Weymann, R. J. 1994, in preparation
Mathewson, D. S., Cleary, M. N., & Murray, J. D. 1974, ApJ, 190, 291
Mathewson, D. S., Schwarz, M. P., & Murray, J. D. 1977, ApJ, 217, L5
McKee, C. F. 1993, in Back to the Galaxy, ed. S. Holt & F. Verter (New York: AIP), in press
McKee, R. X., Newton, L. M., & Morton, D. C. 1983, MNRAS, 205, 1191
Mirabel, I. F., Cohen, R. J., & Davies, R. D. 1979, MNRAS, 186, 433
Morras, R., & Bajaja, E. 1983, A&AS, 51, 131
Morton, D. C. 1991, ApJS, 77, 119
Pettini, M., & West, K. A. 1982, ApJ, 260, 561
Robinson, R. D., Blackwell, J., Feggans, K., Lindler, D., Norman, D., & Shore, S. N. 1992, A User's Guide to the GHRS Software, version 2.0
Russell, S. C., & Bessell, M. S. 1989, ApJ, 70, 865
Savage, B. D. 1988, in QSO Absorption Lines: Probing the Universe, ed. J. C. Blades, D. A. Turnshek, & C. A. Norman (Cambridge: Cambridge Univ. Press), 195
Savage, B. D., & de Boer, K. S. 1979, ApJ, 230, L77
———. 1981, ApJ, 243, 460
Savage, B. D., Jenkins, E. B., Joseph, C. L., & de Boer, K. S. 1989, ApJ, 345, 395
Savage, B. D., et al. 1993a, ApJ, 413, 116
Savage, B. D., Lu, L., Weymann, R. J., Morris, S. L., & Gilliland, R. L. 1993b, ApJ, 404, 124
Savage, B. D., & Massa, D. 1987, ApJ, 314, 380
Savage, B. D., & Sembach, K. R. 1991, ApJ, 379, 245
Sembach, K. R., & Savage, B. D. 1992, ApJS, 83, 147
Sembach, K. R., Savage, B. D., & Massa, D. 1991, ApJ, 372, 81
Shapiro, P. R., & Benjamin, R. A. 1991, PASP, 103, 923
Shapiro, P. R., & Field, G. G. 1976, ApJ, 207, 406
Shaver, P. A., McGee, R. X., Newton, L. M., Danks, A. C., & Pottasch, S. R. 1983, MNRAS, 204, 53
Shklovsky, I. S. 1952, Astron. J. USSR, 29, 418
Spitzer, L. 1956, ApJ, 124, 20
———. 1976, Comm. Astrophys., 6, 177
———. 1990, ARA&A, 28, 71
Spitzer, L., & Fitzpatrick, E. L. 1993, ApJ, 409, 299
Sutherland, R. S., & Dopita, M. A. 1993, ApJS, 88, 253
Verschuur, G. L. 1973, A&A, 22, 139
Wakker, B. P. 1991, in IAU Symp. 144, The Interstellar Disk-Halo Connection in Galaxies, ed. H. Bloemen (Dordrecht: Reidel), 27
Wakker, B. P., & Shwarz, U. J. 1991, A&A, 250, 484
Wannier, P., Wrixon, G. T., & Wilson, R. W. 1972, A&A, 18, 224
Weedman, D. W. 1976, ApJ, 208, 30
West, K. A., Pettini, M., Penston, M. V., Blades, J. C., & Morton, D. C. 1985, MNRAS, 215, 481
Wheeler, J. C., Sneden, C., & Truran, J. W., Jr. 1989, ARA&A, 27, 279
Yanny, B., & York, D. G. 1992, ApJ, 391, 569
York, D. G. 1988, in QSO Absorption Lines: Probing the Universe, ed. J. C. Blades, D. A. Turnshek, & C. A. Norman (Cambridge: Cambridge Univ. Press), 227
York, D. G., Dopita, M., Green, R., & Bechtold, J. 1986, ApJ, 311, 610